Full title: Engineered neural tissue with Schwann cell differentiated human dental pulp stem cells: potential for peripheral nerve repair?

Short title: Engineered neural tissue from human dental pulp stem cells

Authors: Kathleen Sanen [a], Wendy Martens [b], Melanie Georgiou [c], Marcel Ameloot [a], Ivo Lambrichts [b], James Phillips [d *]

Affiliations:

[a] Biophysics group, Biomedical Research Institute, Hasselt University, Agoralaan Building C, 3590 Diepenbeek, Belgium

[b] Morphology group, Biomedical Research Institute, Hasselt University, Agoralaan Building C, 3590 Diepenbeek, Belgium

[c] Advanced Centre for Biochemical Engineering, University College London, Bernard Katz building, Gordon Street, London, WC1H 0AH, UK.

[d] Biomaterials & Tissue Engineering, UCL Eastman Dental Institute, University College London, 256 Gray's Inn Road, London WC1X 8LD, UK

*** Corresponding author**: jb.phillips@ucl.ac.uk, Phone: +44 (0)20 3456 1254. Fax: +44 (0)20 3456 1227

Keywords (4-6):

- Peripheral nerve injury
- Human dental pulp stem cells
- Schwann cells
- Angiogenesis
- Neurite regeneration
- Nerve tissue engineering

Abstract

Despite the spontaneous regenerative capacity of the peripheral nervous system (PNS), large gap peripheral nerve injuries (PNI) require bridging strategies. The limitations and suboptimal results obtained with autografts or hollow nerve conduits in the clinic urge the need for alternative treatments. Recently, we have described promising neuroregenerative capacities of Schwann cells derived from differentiated human dental pulp stem cells (d-hDPSCs) *in vitro*. Here, we extended the *in vitro* assays to show the pro-angiogenic effects of d-hDPSCs such as enhanced endothelial cell proliferation, migration and differentiation. In addition, for the first time we evaluated the performance of d-hDPSCs in an *in vivo* rat model of PNI. Eight weeks after transplantation of NeuraWrap™ conduits filled with engineered neural tissue containing aligned d-hDPSCs in 15 mm rat sciatic nerve defects, immunohistochemistry and ultrastructural analysis revealed ingrowing neurites, myelinated nerve fibers and blood vessels along the construct. Although further research is required to optimize the delivery of this engineered neural tissue, our findings suggest that d-hDPSCs are able to exert a positive effect in the regeneration of nerve tissue *in vivo*.

1 Introduction

Peripheral nerve injury (PNI) represents a major clinical concern worldwide and has significant socio-economic impact, causing pain and restriction in daily activities of affected individuals. Although endogenous peripheral nerve regeneration is possible, it is a slow and therefore often an incomplete process (Faroni *et al.*, 2015). Many attempts have been made to accelerate neural regeneration and improve functional outcomes. The preferred therapy for PNI is primary end-to-end suturing. However, for large nerve gaps, when tension-free joining of the proximal and distal nerve stumps is excluded, autologous nerve grafting is regarded as the gold standard therapy (Gordon *et al.*, 2011, Millesi, 2007). Nerve autografts provide aligned autologous denervated Schwann cells in an aligned extracellular matrix, the predominant structural component of which is collagen type I. Nevertheless, since morphometric mismatch between graft and native nerve is a frequent occurrence, optimal recovery is often restrained (Nichols *et al.*, 2004). Furthermore, autografting raises additional problems such as donor site morbidity, limited availability of donor tissue and extra time and cost of the second surgical procedure (Siemionow and Brzezicki, 2009). In search for alternative strategies to treat PNI, a wide range of natural and synthetic biomaterials have been developed, with collagen type I being the most commonly used natural polymer, and combined with Schwann cells or stem cells in order to mimic the key features of the autograft (Angius *et al.*, 2012, Bell and Haycock, 2012, Nectow *et al.*, 2012).

In the development of artificial nerve tissue, the use of a cellular scaffold provides an opportunity to promote axon regeneration, vascularization and myelination which are important contributors to functional recovery. Numerous techniques have been applied to recreate the highly oriented cellular and extracellular matrix architecture of peripheral

nerves. Gravity or pressure-driven flow, magnetic fields and electrical gradients can establish alignment of collagen type I fibrils in hydrogels (Jang *et al.*, 2015). Instead of relying on external forces to orient the extracellular matrix, a recent technique described the self-alignment of Schwann cells by using a uniaxially tethered cellular hydrogel system, and as a result collagen fibril alignment (Georgiou *et al.*, 2013). Following plastic compression to stabilize the construct, the resulting engineered neural tissue (EngNT) has been shown to support and guide neuronal growth both *in vitro* and *in vivo* when seeded with rat Schwann cells (Georgiou *et al.*, 2013). To facilitate clinical translation of this potential therapy for PNI, the use of an autologous cell source is preferred. Despite the apparent ideal profile of autologous Schwann cells, their isolation is rather invasive and their expansion is difficult. Furthermore, to obtain alignment of cells in constrained hydrogels, cells need to be able to exert a sufficient level of traction forces, a characteristic that is limited in primary glial cell cultures (East *et al.*, 2010, O'Rourke *et al.*, 2015). In search of alternative cell sources, mesenchymal stem cells have shown to be promising candidates for regenerative medicine purposes.

Dental pulp stem cells (DPSCs) represent an easily accessible source of adult stem cells as they can be isolated from extracted wisdom teeth (Gronthos *et al.*, 2000). The proliferative and immunomodulatory properties of DPSCs are more pronounced compared to bone marrow-derived mesenchymal stem cells (Pierdomenico *et al.*, 2005), which enforces their therapeutic potential. Furthermore, their neural crest origin has triggered extensive research on the neurogenic differentiation potential of DPSCs (Tatullo *et al.*, 2015). Recently, we described the *in vitro* differentiation of human DPSCs (hDPSCs) towards Schwann-like cells (d-hDPSCs) (Martens *et al.*, 2014). In addition to successful morphological differentiation, the *in vitro* functionality of d-

hDPSCs was confirmed as they not only promoted neuronal survival, but also directed neurite outgrowth and myelinated axons in self-aligned 3D co-cultures. These promising data are a first indication that d-hDPSCs could be used as an alternative Schwann cell source for the construction of artificial neural tissue for the treatment of PNI. However, additional research is required in order to potentiate therapeutic application of d-hDPSCs. Since the survival of transplanted cells in bioengineered scaffolds depends, amongst others, on adequate (neo-) vascularization of the construct, a cell population with an angiogenic profile could have therapeutic benefits. Only recently, the positive impact of hDPSCs on endothelial cell proliferation and tube formation was described (Hilkens *et al.*, 2014). In addition, both the capillary density of skeletal muscles and intra-epidermal nerve fiber density of diabetic rats was significantly ameliorated upon transplantation of DPSCs into skeletal muscles (Hata *et al.*, 2015).

Within the current study, we investigated the initial use of d-hDPSCs as a cell-based therapy for peripheral nerve repair. First, the paracrine angiogenic properties of d-hDPSCs were investigated at the level of endothelial proliferation, migration and tube formation. Next, EngNT constructs containing d-hDPSCs (EngNT_d-hDPSC) were transplanted within a NeuraWrap™ conduit in an *in vivo* rat model of large gap PNI and the regenerated nerve tissue was evaluated for the presence of neurites, myelinated axons and blood vessels.

2 Materials and methods

2.1 Materials and products

All products were purchased from Sigma-Aldrich (Bornem, Belgium) unless stated otherwise.

2.2 Cell culture

Human third molars were collected from donors (15-20 years of age) undergoing extraction for orthodontic or therapeutic reasons at Ziekenhuis Oost-Limburg, Genk, Belgium. The medical ethical committee of Ziekenhuis Oost-Limburg approved this study and written informed consent from all donors, or from legal guardians in case of under-aged donors, was obtained. hDPSCs were isolated and differentiated towards Schwann-like cells (d-hDPSCs) in 2D conditions as described previously (Martens *et al.*, 2014). hDPSCs were maintained in minimal essential medium, α modification (αMEM) supplemented with 10% fetal bovine serum (FBS, Biochrom AG, Berlin, Germany), 2 mM L-glutamine, 100 U/ml penicillin, and 100 µg/ml streptomycin, further referred to as standard culture medium. After the induction of differentiation, d-hDPSCs were cultured in complete differentiation medium, which is standard culture medium supplemented with 5 µM forskolin, 10 ng/ml basic fibroblast growth factor, 5 ng/ml platelet-derived growth factor AA, and 200 ng/ml heregulin-β-1 (Immunotools, Friesoythe, Germany).

A human microvascular endothelial cell line (HMEC-1) was purchased from the Center of Disease Control and Prevention (Atlanta, GA). The cells were cultured in MCDB 131 medium (Invitrogen, Carlsbad, CA) supplemented with 100 U/ml Penicillin and 100

µg/ml Streptomycin, 10 mM L-glutamine, 10% FBS, 10 ng/ml human epidermal growth factor (hEGF, Immunotools, Germany) and 1 µg/ml hydrocortisone (Immunotools).

2.3 Collection of conditioned medium and ELISA

Donor-matched hDPSCs or d-hDPSCs were seeded at a density of 20,000 cells/cm^2 in standard or complete differentiation culture medium respectively. After 24 h, cells were washed 3 times in phosphate buffered saline (PBS) and fed fresh standard culture medium containing 0.1% FBS. Another 48 h later, the medium was collected and stored at -80°C.

An enzyme-linked immunosorbent assay (ELISA) was performed according to the manufacturer's protocol on conditioned medium from 4 different donors in order to determine the concentration of VEGF-A produced by hDPSCs and d-hDPSCs (RayBiotech, Inc., Boechout, Belgium). Experiments were performed in triplicate and absorbance was measured at 450 nm by means of the FLUOstar Optima multifunctional microplate reader (BMG Labtech, Germany).

2.4 Alamar Blue cell proliferation assay

HMEC-1 were seeded in a 96-well plate at a density of 10,000 cells per well in standard MBEC culture medium. After attachment to the culture plate, cells were rinsed with PBS and incubated with conditioned medium from hDPSCs or d-hDPSCs for 24, 48 or 72 h. αMEM with 0.1% FBS was used as negative control. Alamar Blue ® Cell Viability Reagent (Invitrogen, Carlsbad, CA) was added 4 h prior to readout according to the manufacturer's instructions.

2.5 Transwell migration assay

HMEC-1 were seeded in tissue culture inserts (ThinCertTM, 8 µm pore size, Greiner Bio-One, Frickenhausen, Germany) at 100,000 cells/cm² in standard hDPSC culture medium containing 0.1% FBS and placed into a 24-well plate. Underneath the tissue culture inserts, conditioned medium from hDPSCs or d-hDPSCs was added. Standard hDPSC culture medium containing 10% FBS or 0.1% FBS was used as a positive and negative control respectively. Following 24h of incubation, transmigrated HMEC-1 were fixed with 4% paraformaldehyde (PFA) in PBS and stained with 0.1% crystal violet in 70% ethanol. Cells on the surface of the upper chamber were gently removed with a cotton swab. Per insert, two representative pictures were taken with an inverted phase-contrast microscope (Nikon Eclipse TS100, Nikon co., Japan) equipped with a ProgRes® C3 digital microscope camera (Jenoptik AG, Jena, Germany). The amount of migration (segmentation based on stained cells expressed as mean area percent) was quantified using AxioVision software 4.6.3 (Carl Zeiss Vision, Aalen, Germany).

2.6 Tube formation assay

In order to evaluate the effect of hDPSCs and d-hDPSCs on tubulogenesis, a tube formation assay (*in vitro* angiogenesis assay kit, Millipore) was performed. ECMatrix^{TM} was prepared in 96-well plates as described by the manufacturer, and 15,000 HMEC-1 were plated onto the surface in the presence of conditioned medium from hDPSCs or d-hDPSCs. Standard hDPSCs culture medium containing 10% FBS and 0.1% FBS was used as a positive and negative control, respectively. HMEC-1 were allowed to attach for 4 h before tube formation was evaluated using the inverted phase-contrast microscope described above. Three random fields from each well were captured and analyzed using Angiogenesis Analyzer (ImageJ) for the number of branching points,

total network length (continuously joined end-end cells) and the number of closed polygon-shaped structures (mesh size).

2.7 Preparation of EngNT_d-hDPSCs

Gels were prepared as described previously (Martens *et al.*, 2014) with some modifications. Tethered gels were kept in standard culture medium at 37 °C in a humidified atmosphere containing 5% CO_2 for 24 h to allow alignment of d-hDPSCs, after which they were stabilised by plastic compression (Brown *et al.*, 2005). The resulting 40 μm thick sheets of EngNT_d-hDPSCs were rolled up to form rods (approximately 200 μm diameter × 15 mm length) and kept in standard culture medium until transplantation into an animal model of sciatic nerve injury later the same day.

2.8 Surgical repair of rat sciatic nerve

All experimental procedures involving animals were conducted in accordance with the UK Animals (Scientific Procedures) Act (1986)/the European Communities Council Directives (86/609/EEC) and approved by the Open University Animal Ethics Advisory Group. Surgery on Sprague Dawley (250–500 g) rats was performed as described previously (Georgiou *et al.*, 2015). To assess neuronal regeneration across a 15 mm gap, three groups (7 rats per group) were included: (A) empty NeuraWrap™ conduit (18 mm long with 1.5 mm at each end to accommodate proximal and distal stump), (B) two EngNT_d-hDPSCs rods (15 mm long) in a NeuraWrap™ sheath (18 mm long) or (C) a 15 mm nerve graft taken from a littermate culled using CO_2 asphyxiation (allograft). Animals receiving d-hDPSCs were immunosuppressed by sub-cutaneous injection of Cyclosporine A (15 mg/kg) 24 h prior to the surgery and then daily throughout the recovery period. After 8 weeks, animals were culled using CO_2 asphyxiation and

repaired nerves were excised and immersion fixed in 4% PFA at 4°C. The central 3 mm of the repair device was removed and prepared for transmission electron microscopy (TEM) and transverse cryostat sections (10 µm thick) were prepared from the proximal and distal parts of the device and the nerve stumps for immunostaining (**Figure 5a**).

2.9 Transmission electron microscopy

Following fixation with 4% PFA, the fixative was gently aspirated with a glass pipette, and tissues from the central 3 mm of the repair devices were postfixed in 2% osmium tetroxide (Aurion) for 1 h. Subsequently, tissues were dehydrated through a series of graded concentrations of acetone and embedded in araldite according to the popoff method (Bretschneider *et al.*, 1981). Semi-thin sections (0.5 µm) were stained with toluidine blue after which they were scanned with a Mirax digital slide scanner (Carl Zeiss Vision, Aalen, Germany). Ultrathin sections (0.06 µm) were mounted, contrasted and examined as described previously (Martens *et al.*, 2014). The images were processed digitally with iTEM-FEI software (Olympus SIS). The number of blood vessels and myelinated neurites in the whole of each cross-section was quantified manually.

2.10 Immunostaining

Prior to the staining, cryosections from the proximal and distal parts of the device and the nerve stumps were washed with PBS and post-fixed in 4% PFA for 10 min at room temperature (RT). Sections were permeabilized with 0.05% Triton-X for 30 min at 4°C and blocked using 5% normal donkey serum in PBS for 30 min at RT. A mouse monoclonal anti-neurofilament antibody (1:100, DakoCytomation, Glostrup, Denmark) was diluted in 0.2% Triton-X and incubated overnight at 4°C. As secondary antibody,

donkey anti-mouse labeled with A555 (1:500, Invitrogen/Molecular probes, Merelbeke, Belgium) was applied for 45 min at RT in the dark. Following nuclear counterstaining using 4',6-diamidino-2-phenylindole (DAPI), slides were mounted with fluorescent mounting medium (Dako, Glostrup, Denmark). Images were taken with a Nikon Eclipse 80i fluorescence microscope equipped with a Nikon digital sight camera DS-2MBWc (Nikon, Tokyo, Japan). Primary antibody was omitted in the negative control condition. To assess axonal growth throughout the EngNT, the total number of neurites was quantified. Pictures were taken covering the whole section and NF-positive neurites were counted manually using Image J software (NIH; available at: http://rsb.info.nih.gov/ij/).

2.11 Confocal microscopy

To quantify the density of NF growth within the EngNT group, high quality overview images were obtained from cryosections, mapping the entire cross-section of the mid-proximal part (Figure 5a). Imaging was performed using a Zeiss LSM510 META (Carl Zeiss, Jena, Germany) mounted on an Axiovert 200M and a 40x/1.1 water immersion objective (LD C-Apochromat 40/1.1W Korr UV-VIS-IR, Carl Zeiss), yielding a pixel size of 0.439 µm. The Alexa 555 fluorophore was excited with the 543 nm emission line of a He-Ne laser and internally detected after a 560 nm long pass filter. DAPI excitation was achieved by two-photon excitation at 720 nm performed by a MaiTai laser (Spectra- Physics, CA, USA) and when transmitted through a 37.5 nm wide band pass filter with a central wavelength of 427.5 nm, emitted light was captured by an analogue photomultiplier tube (Zeiss). Confocal z-stacks were acquired (depth 9 µm, z-resolution 0.89 µm), and tiled together to produce a mosaic of image z-stacks that spanned the entire cryosection. 3D images were compressed to a single image using Image J. Next,

sections were subdivided into three zones (EngNT_d-hDPSCs material; 25 µm border around each EngNT_d-hDPSCs rod; remaining area within conduit) to assess the location of neurites in relation to the EngNT_d-hDPSCs. The density of neurites in each zone was measured using Image J software analysis and expressed as mean grey value.

2.12 Statistical analysis

Statistical analysis was performed using GraphPad Prism 5 software (GraphPad, San Diego, CA, USA). Data from the VEGF-A ELISA were submitted to a D'Agostino-Pearson omnibus normality test, followed by an unpaired t test. Data from the proliferation assay, neurofilament stainings were compared by means of a 2-way ANOVA followed by Bonferroni's multiple comparison test. Data from the migration and tube formation assay and the blood vessel and myelin counting were first controlled for normality by means of a D'Agostino-Pearson omnibus normality test, followed by comparison of control and experimental groups by means of a Kruskal-Wallis test while applying a Dunn's multiple comparison *post hoc* test. Values of $P \leq 0.05$ were considered statistically significant. All data are expressed as means ± standard error of mean (SEM).

3 Results

3.1 Expression of VEGF-A by hDPSCs and d-hDPSCs *in vitro*

In our previous study (Martens *et al.*, 2014), we identified a range of neurotrophic factors which are differentially expressed by d-hDPSCs compared to hDPSCs. Here, we evaluated the expression level of the angiogenic factor VEGF-A between both cell populations. ELISA revealed that d-hDPSCs secreted a significantly higher concentration of VEGF-A compared to hDPSCs (**Figure 1**).

3.2 Angiogenic properties of d-hDPSCs *in vitro*

Angiogenesis is a well-coordinated process involving endothelial cell proliferation, migration and differentiation. Therefore, the potential effects of factors secreted by d-hDPSCs on each of these endothelial cell behaviors were evaluated using a series of *in vitro* assays. First, the proliferation-promoting capacity of d-hDPSCs was evaluated using an Alamar Blue assay. The results in **Figure 2** show that after 72 h, the endothelial cell line HMEC-1 had proliferated significantly more in the presence of conditioned medium from hDPSCs and d-hDPSCs compared to those in control medium.

Since endothelial cells can migrate in response to chemical stimuli, the chemotactic potential of d-hDPSCs was examined. In the transwell migration assay, HMEC-1 showed significantly increased transmigration in the presence of conditioned medium from hDPSCs and d-hDPSCs compared to those in control medium (**Figure 3**).

Finally, an ECMatrix™ assay was performed to assess the effect of d-hDPSCs on endothelial tube formation. Following 4 h incubation of HMEC-1 seeded in ECMatrix™, the conditioned medium of hDPSCs or d-hDPSCs significantly increased

the number of nodes, segments and meshes compared to control medium (**Figure 4a-d**). Furthermore, the total branching length of endothelial tubes was significantly longer in these conditions compared to the negative control (**Figure 4e**).

3.3 Nerve repair

d-hDPSCs were seeded in uniaxial tethered collagen type I hydrogels. Following cellular self-alignment, the gels were stabilized by plastic compression and rolled into rods, of which two were placed within NeuraWrap™ conduits. Adult rats with a 15 mm sciatic nerve gap received either EngNT_d-hDPSCs, empty conduit or allograft transplants. Following an 8 week recovery period, specific parts of the excised transplants were processed for transverse cryosectioning and subsequent immunofluorescence staining to detect neurofilament (**Figure 5a**). For each group, the number of neurites in the mid-proximal and mid-distal part of the construct were normalized to the number of neurites in the proximal nerve stump, which was set at 100% (**Figure 5b**). In the empty conduit group, only about half of the neurites reached the mid-proximal part of the construct (54.2 ± 8.4%), which was significantly fewer compared to the allograft group (85.4 ± 6.8%). The number of neurites in the EngNT_d-hDPSCs group at this level was 78.3 ± 7.5% of the neurites in the proximal stump. In the mid-distal part of the transplants, the level of neurite regeneration in the allograft group was approximately 2.5-fold higher than the EngNT and empty conduit groups. In order to capture the transverse distribution of regeneration within the EngNT_d-hDPSCs constructs, the density of neurites in three different zones within the mid-proximal part was determined: zone 1 comprised the EngNT_d-hDPSCs rods, a border of 25 µm adjacent to the rod defined zone 2 and the remainder of the construct lumen (NeuraWrap™ excluded) was zone 3 (**Figure 5c**). No significant differences between

the three zones were observed, although zone 2 showed a trend for higher mean grey values (relative to the density of neurofilament immunoreactivity) compared to the other zones (**Figure 5d**).

3.4 Blood vessels and myelin

The mid part of the excised transplants (**Figure 5a**, dark grey) were processed for TEM. The analysis of semi-thin sections stained with toluidine blue revealed regenerated nerve tissue throughout the cross-section of the allograft group, the presence of 2 rods and regenerated tissue in the EngNT_d-hDPSCs samples and limited tissue regeneration in the empty conduit group (**Figure 6a**, upper part). At the ultrastructural level (**Figure 6a**, lower part), blood vessels and myelinated nerves in the EngNT_d-hDPSCs group were observed within and near an abundant fibrillar extracellular matrix. Although blood vessels and myelinated nerve fibers were also present in the empty conduit samples, collagen type I fibrils were hardly detectable. The numbers of blood vessels and of myelinated fibers were assessed for the whole area of each tissue section (**Figure 6b-c**). The allograft and EngNT_d-hDPSCs groups contained significantly more blood vessels compared to the empty conduit group. The number of myelinated neurites was significantly higher in the allograft group, but there was no difference in this measure between the EngNT_d-hDPSCs and empty conduit group. The great majority of vessels appeared to be oriented longitudinally along the constructs, which may be beneficial for supporting or guiding neuronal regeneration. Although no correlation was observed between the number of blood vessels and the number of myelinated neurites for any of the groups, the three experimental groups seemed to exhibit different characteristic patterns with regard to numbers of blood vessels and myelinated neurites (**Figure 6d**). Overall, the empty conduit group had low blood vessel and low myelin counts, the

EngNT_d-hDPSCs group had high blood vessel and low myelin counts and the allograft showed both high blood vessel and high myelin counts.

4 Discussion

A major challenge in the field of neuroscience is the repair of peripheral nerve gaps. In the clinic, different strategies such as autografts, allografts and nerve conduits are employed to join nerve ends and enhance PNS regeneration (Chiono and Tonda-Turo, 2015). Unfortunately, repair outcomes of these bridging approaches are suboptimal (Grinsell and Keating, 2014). Over the past decades, tissue engineering strategies have been proposed as promising alternatives to reconstruct peripheral nerve defects. A variety of cells and biomaterials have been combined in attempts to provide an adequate environment for nerve regeneration (Rice *et al.*, 2013). As we previously described, d-hDPSCs display neuroprotective and neurotrophic properties, can self-align within collagen type I hydrogels and myelinate neurites *in vitro* (Martens *et al.*, 2014). In the present study, we assessed the angiogenic properties of d-hDPSCs using *in vitro* assays, then a rat sciatic nerve model of PNI was performed for the first time to further understand the potential for using EngNT containing d-hDPSCs as a regenerative strategy for peripheral nerve lesions.

In the first part of this study, the presence of the pro-angiogenic factor VEGF-A in the conditioned medium of hDPSCs and d-hDPSCs was determined via an ELISA. The results showed that d-hDPSCs secreted approximately 2–fold more VEGF-A compared to hDPSCs. VEGF-A is known to stimulate different steps in the process of blood vessel formation, and while it is one of the key factors associated with angiogenesis there are many others that are likely to play a role in mediating the effects of hDPSCs and d-hDPSCs on endothelial cells. Recently, research performed by Hilkens *et al.* showed that hDPSCs had a predominant pro-angiogenic impact on endothelial cell migration

and tube formation (Hilkens *et al.*, 2014), which is confirmed in our study. In addition, we demonstrate that d-hDPSCs have comparable capacities in stimulating the migratory and tubulogenic actions of endothelial cells, indicating that hDPSCs retain their pronounced angiogenic properties following differentiation into Schwann-like cells. Whereas the former publication showed no effect of hDPSCs on endothelial cell proliferation using an MTT (3-(4,5-dimethylthiazol-2-yl)-2,5-diphenyltetrazolium bromide) assay (Hilkens *et al.*, 2014), we observed a significant increase in HMEC-1 when incubated with conditioned medium from hDPSCs or d-hDPSCs for 72 h via an Alamar Blue assay. A possible explanation for this discrepancy could lie in the sensitivity of the conducted proliferation assays, since the fluorescence-based readout of the Alamar Blue assay has been reported to provide higher sensitivity compared to the absorbance measurements obtained by MTT assays (Hamid *et al.*, 2004, Patel *et al.*, 2013). Since several studies have indicated beneficial effects of MSCs on the proliferative capacity of endothelial cells (Duffy *et al.*, 2009, Gruber *et al.*, 2005, Iohara *et al.*, 2008, Potapova *et al.*, 2007) and the results obtained for hDPSCs so far are contradictory, it would be of interest to re-evaluate their effect on endothelial cell proliferation. To circumvent interpretation bias of the aforementioned assays due to metabolic changes in HMEC-1 behavior (Rampersad, 2012), it might be better to conduct future proliferation experiments by means of a Bromodeoxyuridine ELISA (Yadav *et al.*, 2014).

Whilst both hDPSCs and d-hDPSCs promote angiogenesis, only d-hDPSCs were used in the *in vivo* study given their neurotrophic properties and their lineage commitment prior to transplantation (Martens *et al.*, 2014). The capacity of EngNT_d-hDPSCs to support neuronal growth from the proximal stump *in vivo* was assessed in a rat sciatic

nerve injury model. A nerve gap of 15 mm was reconstructed with either nerve allograft, empty conduit or EngNT_d-hDPSCs. Eight weeks after transplantation, immunohistochemical analysis of the mid-proximal part of the allograft and EngNT_d-hDPSCs constructs revealed comparable neuronal regeneration, whereas less neuronal tissue was observed in the empty conduit treated animals. Regeneration was maintained in distal parts of the allograft, whereas in the EngNT_d-hDPSCs transplants the number of neurites in mid-distal regions were lower than in allografts and similar to that of empty conduit transplants. Interestingly, this trend is in contrast to previous research performed with Schwann cells and with differentiated rat adipose-derived stem cells in EngNT, where regeneration was maintained between proximal and distal parts of the implanted constructs (Georgiou *et al.*, 2015). This difference might be attributed to immunosuppressant treatment, administered daily to all the animals in our study and not used in the previous studies where rat cells were used in EngNT. Although hDPSCs have been described to exhibit potent immunomodulatory and anti-inflammatory capacities (Pierdomenico *et al.*, 2005, Tomic *et al.*, 2011), graft-versus-host responses in rats receiving EngNT_d-hDPSCs transplants could not be excluded, so all animals were treated with Cyclosporine A in this study. Both innate and adaptive immune cells have been shown to play a role in clearing myelin and axonal debris and promoting neurite outgrowth (Benowitz and Popovich, 2011), and Namavari *et al.* showed that immunomodulation with Cyclosporine A delays axonal sprouting and growth of transected nerves (Namavari *et al.*, 2012). The recovery period used here of 8 weeks is relatively short for a 15 mm rat sciatic nerve gap, but it facilitates the detection of differences between the allograft and artificial repair constructs which may be reduced if the recovery time is extended. This time point of 8 weeks and gap length of 15 mm

has been established previously to be ‘critical-length’ (Georgiou *et al.*, 2013) and is useful for pre-clinical evaluation of nerve repair conduits (Georgiou *et al.*, 2015).

With regard to the distribution of the regenerating neurites in the EngNT transplants, there was a trend for higher axon densities in the zone directly adjacent to the EngNT rods compared to the surrounding area, which was also a region of high neurite density in the previous study using rat Schwann cells in EngNT (Georgiou *et al.*, 2013). Since neuronal growth within the rods was lower in this study, one could speculate that the longitudinal permeability of the EngNT_d-hDPSCs rods was not optimal for neurite ingrowth. In order to fully exploit the potential of EngNT_d-hDPSCs, other ways of incorporating EngNT sheets within the constructs will be examined in the future. For example, a low density hydrogel could be used as a core material to wrap the EngNT_d-hDPSCs sheets around, or as an additional spacing layer within the rods. By increasing the total available EngNT_d-hDPSCs sheet surface for regenerating axons and facilitating diffusion of neurotrophic factors produced by d-hDPSCs, the growth of neurites into and throughout such constructs might be enhanced.

In the mid part of the construct, the number of blood vessels observed in the EngNT_d-hDPSCs and allograft transplants were comparable. Revascularization of nerve grafts, and especially vascular ingrowth from the surrounding tissue bed, is important since ischemia-induced necrosis and fibrosis hamper axonal regeneration (D’Arpa *et al.*, 2015). Furthermore, transplantation of adipose-derived stem cells has been shown to boost vascularization of the nerve defect (Kingham *et al.*, 2014), which can promote the longevity of the construct. Upon transplantation of EngNT_d-hDPSCs, a lack of intrinsic vascular supply creates a hypoxic environment for the encapsulated cells, thereby triggering the upregulation of pro-angiogenic pathways (Krock *et al.*, 2011).

Because the resulting enhanced vasculature will increase survival chances of the transplanted cells, this is an important component in the provision of subsequent neurotrophic support. The difference in number of regenerated axons between the mid-proximal and the mid-distal part of the EngNT_d-hDPSCs constructs indicates that priority may have given to revascularization and, as a consequence, reinnervation was delayed when compared to allograft controls. Previous studies have demonstrated that longitudinal inosculation is the primary method of revascularisation in allografts, whereby anastomosis occurs between the vessels in the graft and the repaired nerve, accelerating restoration of blood flow without the requirement for angiogenesis (Best *et al.*, 1999, Chalfoun *et al.*, 2003). Given the importance of microvessels in guiding nerve renegeration and supporting neuronal survival (Bearden and Segal, 2004), future improvements to EngNT_d-hDPSCs devices could therefore focus on provision of structures that accelerate vascularisation and promote the survival and neurotrophic behaviour of the implanted cells. In addition, it would be relevant to investigate the fate and phenotype of the differentiated cells over the first days to weeks after transplantation.

In this first study to report the transplantation of human cells in EngNT constructs for peripheral nerve repair, the proximal part of the EngNT_d-hDPSCs showed a comparable amount of neurite regeneration compared to allograft treatment but a lower number of neurites had traversed into the distal part after 8 weeks. This pattern of nerve regeneration was associated with increased vascularisation compared to empty conduits, which was consistent with the pro-angiogenic effects of d-hDPSCs observed *in vitro*. In conclusion, EngNT_d-hDPSCs is a promising new approach that showed an ability to enhance vascularisation and to promote initial neurite ingrowth in a long-gap nerve

repair scenario. Future work will focus on tuning the cell and material environment to improve regeneration in the distal part of the constructs.

5 Acknowledgements

The authors are grateful to Dr. Constantinus Politis and Dr. Luc Vrielinck (Ziekenhuis Oost Limburg, Genk, Belgium) for providing dental pulp tissue, to Marc Jans for excellent tissue processing for transmission electron microscopy and to Open University Biomedical Research Unit staff for post-surgical animal care. K.S. acknowledges fellowship funding from Research Foundation Flanders [Fonds Wetenschappelijk Onderzoek (FWO), grant 11N0914N] and a travel grant *via* the Boehringer Ingelheim Fonds. W.M. benefits from a grant via FWO (GO29112FWO). M.A. acknowledges the Federal Science Policy of Belgium (IAP-7/05), the support by the FWO-onderzoeksgemeenschap ‘‘Scanning and Wide Field Microscopy of (Bio)-organic Systems’’ and the Province of Limburg (Belgium) for the financial support within the tUL IMPULS FASE II program, allowing for the upgrading of the laser source used in this work.

6 Bibliography

Angius D, Wang H, Spinner RJ *et al.* 2012; A systematic review of animal models used to study nerve regeneration in tissue-engineered scaffolds. *Biomaterials*. **33**;(32):8034-9.

Bearden SE, Segal SS. 2004; Microvessels promote motor nerve survival and regeneration through local VEGF release following ectopic reattachment. *Microcirculation*. **11**;(8):633-44.

Bell JH, Haycock JW. 2012; Next generation nerve guides: materials, fabrication, growth factors, and cell delivery. *Tissue engineering Part B, Reviews*. **18**;(2):116-28.

Benowitz LI, Popovich PG. 2011; Inflammation and axon regeneration. *Current opinion in neurology*. **24**;(6):577-83.

Best TJ, Mackinnon SE, Midha R *et al.* 1999; Revascularization of peripheral nerve autografts and allografts. *Plastic and reconstructive surgery*. **104**;(1):152-60.

Bretschneider A, Burns W, Morrison A. 1981; "Pop-off" technic. The ultrastructure of paraffin-embedded sections. *American journal of clinical pathology*. **76**;(4):450-3.

Brown RA, Wiseman M, Chuo CB *et al.* 2005; Ultrarapid engineering of biomimetic materials and tissues: Fabrication of nano- and microstructures by plastic compression. *Adv Funct Mater*. **15**;(11):1762-70.

Chalfoun C, Scholz T, Cole MD *et al.* 2003; Primary nerve grafting: A study of revascularization. *Microsurgery*. **23**;(1):60-5.

Chiono V, Tonda-Turo C. 2015; Trends in the design of nerve guidance channels in peripheral nerve tissue engineering. *Progress in neurobiology*.

D'Arpa S, Claes KEY, Stillaert F *et al.* 2015; Vascularized nerve "grafts": just a graft or a worthwhile procedure? *Plast Aesthet Res*. **2**;(4):183-94.

Duffy GP, Ahsan T, O'Brien T *et al.* 2009; Bone marrow-derived mesenchymal stem cells promote angiogenic processes in a time- and dose-dependent manner in vitro. *Tissue engineering Part A*. **15**;(9):2459-70.

East E, de Oliveira DB, Golding JP *et al.* 2010; Alignment of astrocytes increases neuronal growth in three-dimensional collagen gels and is maintained following plastic compression to form a spinal cord repair conduit. *Tissue engineering Part A*. **16**;(10):3173-84.

Faroni A, Mobasseri SA, Kingham PJ *et al.* 2015; Peripheral nerve regeneration: experimental strategies and future perspectives. *Advanced drug delivery reviews*. **82-83**:160-7.

Georgiou M, Bunting SCJ, Davies HA *et al.* 2013; Engineered neural tissue for peripheral nerve repair. *Biomaterials*. **34**;(30):7335-43.

Georgiou M, Golding JP, Loughlin AJ *et al.* 2015; Engineered neural tissue with aligned, differentiated adipose-derived stem cells promotes peripheral nerve regeneration across a critical sized defect in rat sciatic nerve. *Biomaterials*. **37**:242-51.

Gordon T, Tyreman N, Raji MA. 2011; The basis for diminished functional recovery after delayed peripheral nerve repair. *The Journal of neuroscience : the official journal of the Society for Neuroscience*. **31**;(14):5325-34.

Grinsell D, Keating CP. 2014; Peripheral nerve reconstruction after injury: a review of clinical and experimental therapies. *BioMed research international*. **2014**:698256.

Gronthos S, Mankani M, Brahim J *et al.* 2000; Postnatal human dental pulp stem cells (DPSCs) in vitro and in vivo. *Proceedings of the National Academy of Sciences of the United States of America*. **97**;(25):13625-30.

Gruber R, Kandler B, Holzmann P *et al.* 2005; Bone marrow stromal cells can provide a local environment that favors migration and formation of tubular structures of endothelial cells. *Tissue engineering*. **11**;(5-6):896-903.

Hamid R, Rotshteyn Y, Rabadi L *et al.* 2004; Comparison of alamar blue and MTT assays for high through-put screening. *Toxicology in vitro : an international journal published in association with BIBRA*. **18**;(5):703-10.

Hata M, Omi M, Kobayashi Y *et al.* 2015; Transplantation of cultured dental pulp stem cells into the skeletal muscles ameliorated diabetic polyneuropathy: therapeutic plausibility of freshly isolated and cryopreserved dental pulp stem cells. *Stem cell research & therapy*. **6**:162.

Hilkens P, Fanton Y, Martens W *et al.* 2014; Pro-angiogenic impact of dental stem cells in vitro and in vivo. *Stem cell research*. **12**;(3):778-90.

Iohara K, Zheng L, Wake H *et al.* 2008; A novel stem cell source for vasculogenesis in ischemia: subfraction of side population cells from dental pulp. *Stem Cells*. **26**;(9):2408-18.

Jang JM, Tran SH, Na SC *et al.* 2015; Engineering controllable architecture in matrigel for 3D cell alignment. *ACS applied materials & interfaces*. **7**;(4):2183-8.

Kingham PJ, Kolar MK, Novikova LN *et al.* 2014; Stimulating the neurotrophic and angiogenic properties of human adipose-derived stem cells enhances nerve repair. *Stem cells and development*. **23**;(7):741-54.

Krock BL, Skuli N, Simon MC. 2011; Hypoxia-induced angiogenesis: good and evil. *Genes & cancer*. **2**;(12):1117-33.

Martens W, Sanen K, Georgiou M *et al.* 2014; Human dental pulp stem cells can differentiate into Schwann cells and promote and guide neurite outgrowth in an aligned tissue-engineered collagen construct in vitro. *FASEB J*. **28**;(4):1634-43.

Millesi H. 2007; Bridging defects: autologous nerve grafts. *Acta neurochirurgica Supplement*. **100**:37-8.

Namavari A, Chaudhary S, Chang JH *et al.* 2012; Cyclosporine immunomodulation retards regeneration of surgically transected corneal nerves. *Invest Ophthalmol Vis Sci*. **53**;(2):732-40.

Nectow AR, Marra KG, Kaplan DL. 2012; Biomaterials for the development of peripheral nerve guidance conduits. *Tissue engineering Part B, Reviews*. **18**;(1):40-50.

Nichols CM, Brenner MJ, Fox IK *et al.* 2004; Effects of motor versus sensory nerve grafts on peripheral nerve regeneration. *Exp Neurol*. **190**;(2):347-55.

O'Rourke C, Drake RA, Cameron GW *et al.* 2015; Optimising contraction and alignment of cellular collagen hydrogels to achieve reliable and consistent engineered anisotropic tissue. *Journal of biomaterials applications*.

Patel HD, Zaveri AD, Zaveri DN *et al.* 2013; Comparison of the MTT and Alamar Blue assay for in vitro anti-cancer activity by testing of various chalcone and thiosemicarbazone derivatives. *International Journal of Pharma and Bio Sciences*. **4**;(2):707-16.

Pierdomenico L, Bonsi L, Calvitti M *et al.* 2005; Multipotent mesenchymal stem cells with immunosuppressive activity can be easily isolated from dental pulp. *Transplantation*. **80**;(6):836-42.

Potapova IA, Gaudette GR, Brink PR *et al.* 2007; Mesenchymal stem cells support migration, extracellular matrix invasion, proliferation, and survival of endothelial cells in vitro. *Stem Cells*. **25**;(7):1761-8.

Rampersad SN. 2012; Multiple applications of Alamar Blue as an indicator of metabolic function and cellular health in cell viability bioassays. *Sensors*. **12**;(9):12347-60.

Rice JJ, Martino MM, De Laporte L *et al.* 2013; Engineering the regenerative microenvironment with biomaterials. *Advanced healthcare materials*. **2**;(1):57-71.

Siemionow M, Brzezicki G. 2009; Chapter 8: Current techniques and concepts in peripheral nerve repair. *International review of neurobiology*. **87**:141-72.

Tatullo M, Marrelli M, Shakesheff KM *et al.* 2015; Dental pulp stem cells: function, isolation and applications in regenerative medicine. *J Tissue Eng Regen M*. **9**;(11):1205-16.

Tomic S, Djokic J, Vasilijic S *et al.* 2011; Immunomodulatory properties of mesenchymal stem cells derived from dental pulp and dental follicle are susceptible to activation by toll-like receptor agonists. *Stem cells and development*. **20**;(4):695-708.

Yadav K, Singhal N, Rishi V *et al.* 2014; Cell proliferation assays. *eLS*.

7 Figure captions

Figure 1: Expression of the angiogenic factor VEGF-A by hDPSCs and d-hDPSCs *in vitro*. ELISA indicated a significant increase in VEGF-A release over 48 h *in vitro* after differentiation of hDPSCs toward Schwann cells. Data represent means ± SEM (n = 4). *P < 0.05.

Figure 2: Effect of hDPSCs and d-hDPSCs on endothelial cell proliferation. Endothelial cells were incubated for 24, 48 or 72 h with conditioned medium from hDPSCs or d-hDPSCs. Negative control (neg) is culture medium containing 0.1% FCS. Endothelial cell proliferation was measured using an Alamar Blue fluorescence assay. Data represent means ± SEM (n = 4). P < 0.05 for hDPSCs (*) or d-hDPSCs (#) compared to the negative control at that time point. Error bars may be smaller than the symbol.

Figure 3: Effect of hDPSCs and d-hDPSCs on endothelial cell migration. (a) Representative micrographs show endothelial cell transmigration following 24 h of incubation with conditioned medium from hDPSCs or d-hDPSCs. Culture medium containing 10% FBS or 0.1% FBS was included as positive (pos) and negative (neg) control respectively. Cells were stained with crystal violet. Scale bars = 200 µm. **(b)** Endothelial cell transmigration expressed as the mean percentage area per condition. Data represent means ± SEM (n = 4). *P < 0.05, **P < 0.01.

Figure 4: Effect of hDPSCs and d-hDPSCs on endothelial tubulogenesis. (a) Representative micrographs show endothelial cell tube formation following 4 h of incubation with conditioned medium from hDPSCs or d-hDPSCs. Culture medium containing 10% FBS or 0.1% FBS was included as positive and negative control respectively. Scale bars = 300 µm.

The average number of nodes **(b)**, segments **(c)** and meshes **(d)** and the total branching length **(e)** was measured for each condition. Data represent means ± SEM (n = 4). *P < 0.05, **P < 0.01, ***P < 0.001.

Figure 5: Quantification of nerve regeneration by repair devices and allografts. **(a)** Schematic representation of 15 mm transplanted construct (allograft: n = 7; empty conduit: n = 7; or EngNT_d-hDPSCs: n = 6) with indications on transverse sectioning for post-processing. **(b)** Nerve regeneration throughout the constructs was assessed by means of neurofilament fluorescence staining on transverse cryosections. The number of neurofilament positive axons in the mid-proximal and mid-distal part of the constructs were counted and compared to the number of axons detected in the proximal part of the conduit (expressed as percentage of proximal part). In the proximal part, there were 8675 ± 943 neurites in the allograft group, 8642 ± 1186 neurites in the empty conduit group and 9556 ± 1754 neurites in the EngNT_d-hDPSCs group. The number of nerve fibers is the distal nerve segments were respectively 5489±443, 1520±313 and 2320±549 respectively. **(c)** Schematic representation of transverse section of two EngNT_d-hDPSCs rods in a NeuraWrap™ sheath with indications of different zones within the mid-proximal part in which the number of axons per unit area were quantified: zone 1 = whole EngNT_d-hDPSCs rods; zone 2 = 25 µm adjacent to EngNT_d-hDPSCs rods; zone 3 = rest of the cross-sectional area within the NeuraWrap™ sheath. **(d)** The axon density is represented by the mean grey value of neurofilament fluorescent staining for each zone. Data represent means ± SEM. **P < 0.01, ***P < 0.001.

Figure 6: Comparison number of blood vessels and myelinated fibers. The mid parts of the 15 mm conduits were processed for TEM examination. **(a)** Representative semi-thin (0.5 µm) toluidine blue stained sections (upper row scale bars = 300 µm; lower row scale bars =

100 µm) and TEM images (upper row scale bars = 10 µm; lower row scale bars = 1 µm). Red dotted line marks the edge of a cellular hydrogel rod, and representative higher magnification images of collagen fibrils inside and outside a rod are also shown. The number of blood vessels **(b)** and myelinated neurites **(c)** in the whole of each cross-section were quantified manually. A scatter plot **(d)** depicts the mean number of blood vessels and myelinated neurites for every animal that received allograft, EngNT_d-hDPSCs or empty conduit transplantation. Data represent means ± SEM. *P < 0.05, **P < 0.01.

Figure 1

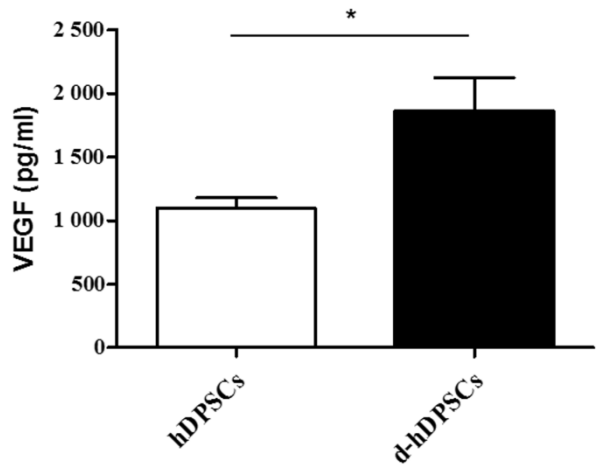

Figure 2

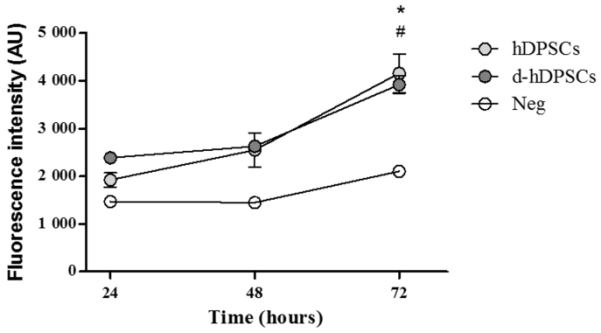

Figure 3

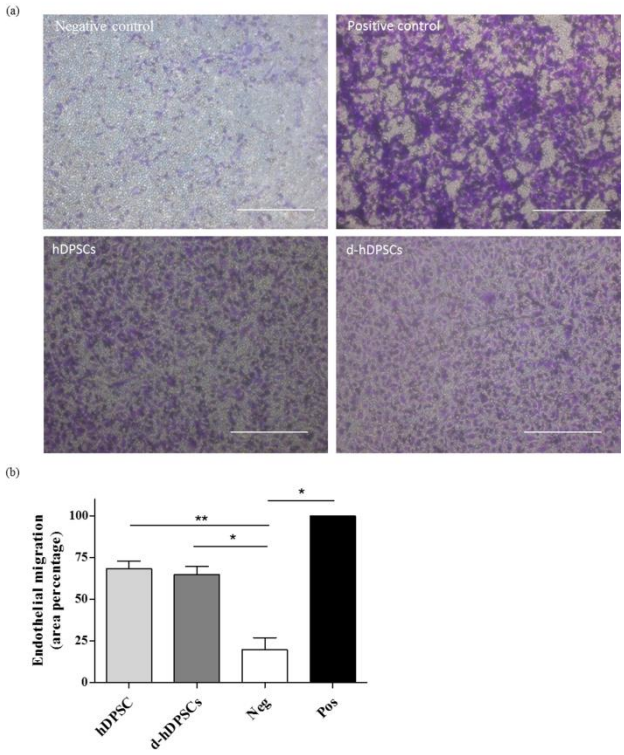

Figure 4

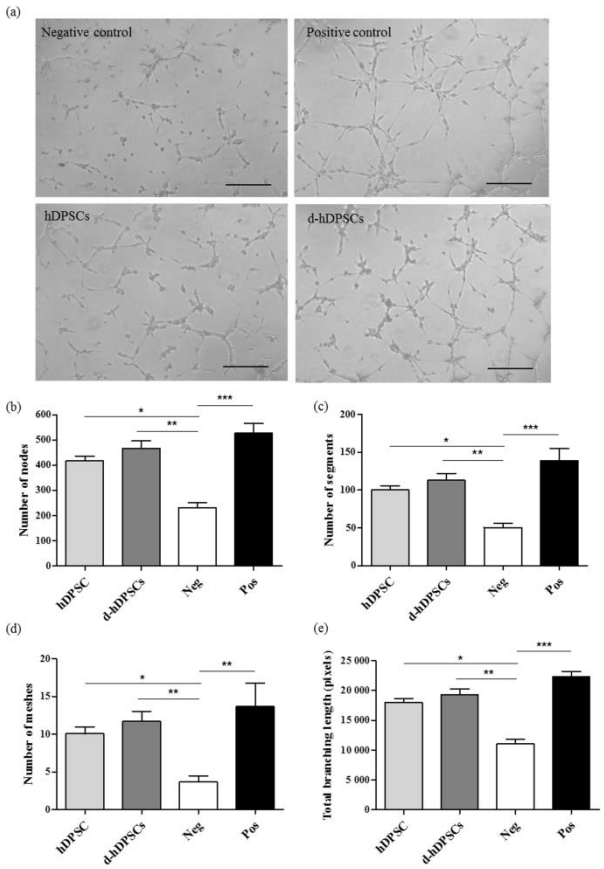

Figure 5

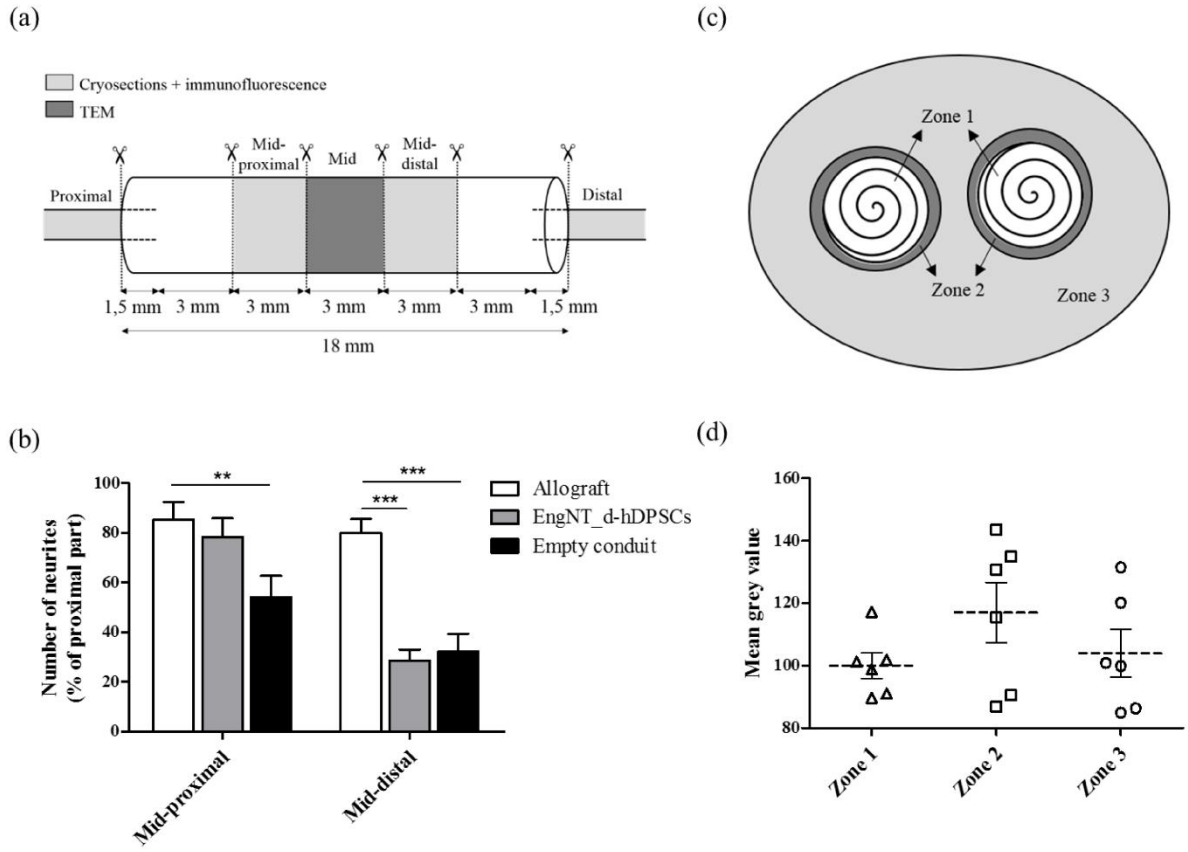
(a)
Cryosections + immunofluorescence
TEM
Mid-proximal
Mid
Mid-distal
Proximal
Distal
1,5 mm
3 mm
3 mm
3 mm
3 mm
3 mm
1,5 mm
18 mm
(c)
Zone 1
Zone 2
Zone 3
(b)
Number of neurites (% of proximal part)
Allograft
EngNT_d-hDPSCs
Empty conduit
**
***
***
Mid-proximal
Mid-distal
(d)
Mean grey value
Zone 1
Zone 2
Zone 3

Figure 6

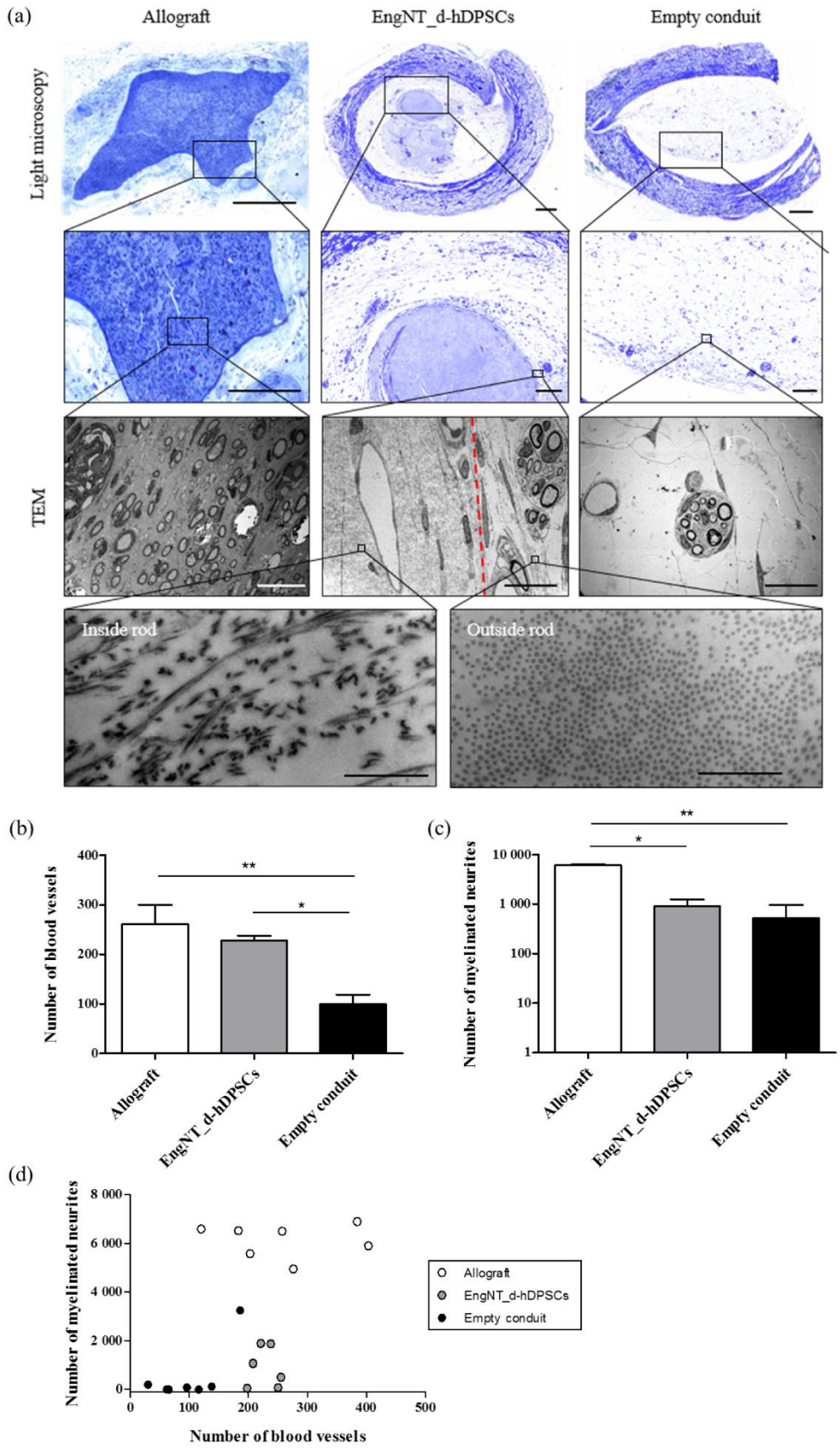
(a)
Allograft
EngNT_d-hDPSCs
Empty conduit
Light microscopy
TEM
Inside rod
Outside rod
(b)
Number of blood vessels
400
300
200
100
0
**
*
Allograft
EngNT_d-hDPSCs
Empty conduit
(c)
Number of myelinated neurites
10 000
1 000
100
10
1
**
*
Allograft
EngNT_d-hDPSCs
Empty conduit
(d)
Number of myelinated neurites
8 000
6 000
4 000
2 000
0
0
100
200
300
400
500
Number of blood vessels
Allograft
EngNT_d-hDPSCs
Empty conduit